Borner et al., http://www.jcb.org/cgi/content/full/jcb.201111049/DC1

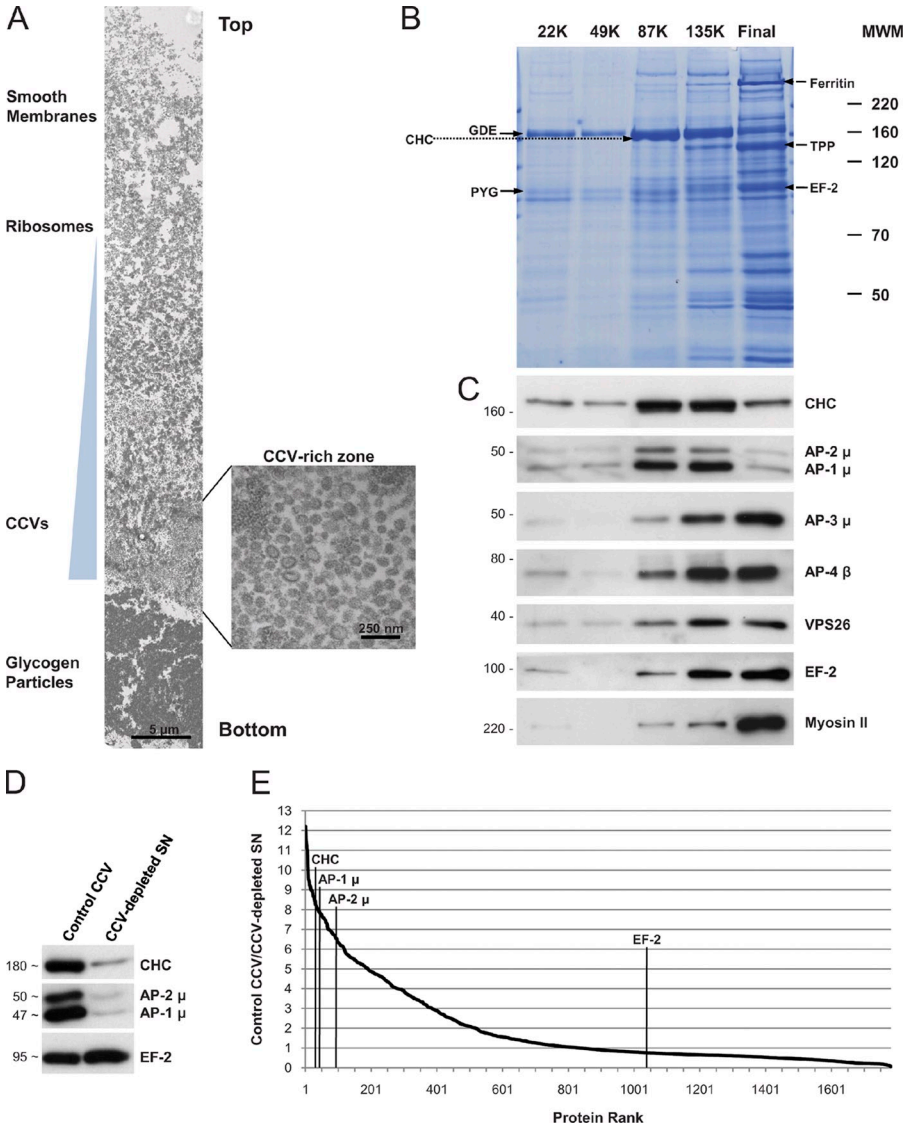

Figure S1. **Analysis of the CCV-enriched fraction by electron microscopy allows the design of an improved preparation protocol.** (A–C) A CCV-enriched subcellular fraction can be prepared from HeLa cells by standard differential centrifugation techniques (originally published in Hirst et al., 2004). The fraction is contaminated with ribosomes, glycogen particles, proteasomes, and other abundant large protein complexes, as well as diverse smooth membrane vesicles (Borner et al., 2006). To improve the purity of the CCV fraction, we refined the final step of the protocol, which is a high-speed spin to pellet CCVs (135,000 *g*, 30 min). (A) First, we analyzed a cross section of the CCV pellet by electron microscopy. The micrograph shows that the pellet is composed of several morphologically distinct layers. The bottom layer consists mostly of glycogen particles, followed by a zone of highly concentrated CCVs (see the magnified field). Further upwards, the concentration of CCVs begins to decline, and ribosomes become more predominant. The top layer of the pellet contains smooth membrane vesicles of different sizes. The different layers indicate the order in which components of the CCV fraction are pelleted: first glycogen, then CCVs, followed by ribosomes and smooth membranes. This observation suggests that the final spin of the CCV preparation may be improved to pellet CCVs more selectively, and hence separate them from contaminants. (B) To determine optimal pelleting conditions, the final step was performed as a series of successive short spins with different speeds (as indicated), with each spin using the supernatant from the preceding spin. Pellets were analyzed by SDS-PAGE. Gels were stained with Coomassie blue, and selected bands were identified by mass spectrometry (arrows). The gel confirms the order in which different components of the CCV fraction pellet. The first two fractions (22K and 49K) contain mostly glycogen-associated proteins (GDE and PYG); clathrin (and thus CCVs) peaks in the 87K and 135K fractions, whereas ribosomal and other contaminants are most effectively pelleted in the "final spin." Speeds of spins are indicated in terms of *g*. All spins were performed for 10 min; the "final spin" was performed at 135,000 *g* for 50 min. Approximate molecular masses are indicated (in kilodaltons). GDE, glycogen debranching enzyme; PYG, glycogen phosphorylase; TPP, tripeptidyl-peptidase 2; EF-2, ribosomal elongation factor 2. (C) The fractions shown in B were analyzed by Western blotting. Consistent with the SDS-PAGE, clathrin peaks in the 87K and 135K fractions, together with the clathrin APs AP-1 and AP-2. The "final spin" is strongly depleted of CCV proteins, and hence not required for effective CCV pelleting. Based on these observations, the CCV preparation was modified to obtain the "improved" CCV fraction (see Materials and methods). Furthermore, C illustrates that the fractionation properties of contaminating membrane vesicles are distinct from those of CCVs: retromer (VPS26), AP-3, and AP-4 are all relatively more abundant than clathrin in the "final spin." This difference can be used to discriminate CCVs from contaminants, as implemented in Fig. 1 (C and F). (D and E) Comparison of control and CCV-depleted fractions allows for the identification of CCV proteins. The final step of the (improved) control CCV fractionation protocol is a high-speed spin (66,500 *g*, 30 min) to pellet CCVs. The spin parameters are optimized to pellet CCVs selectively, and leave a large proportion of contaminating protein particles (e.g., ribosomes and proteasomes) in the supernatant. However, the contaminants may also be pelleted from the supernatant with a higher-speed spin (195,500 *g*, 30 min). The resulting pellet is largely devoid of CCVs. A quantitative comparison of the two fractions identifies candidate CCV proteins as those that are highly enriched in the CCV pellet. (D) Western blots of CCV fractions. (E) Corresponding proteomic analysis by SILAC and quantitative mass spectrometry. The ratio of enrichment in the CCV fraction versus the CCV-depleted fraction was calculated for each protein, and proteins were ranked from the highest to the lowest ratio. AP, AP complex; EF-2, ribosomal elongation factor 2. The experiment is conceptually related to the CCV fractionation shown in Fig. 1 (C and F). The obtained order of proteins is similar, but the ratios of enrichment are higher. This SILAC dataset is annotated as Fractionation "4*" in Fig. 2 and Table S1. Positions of protein molecular mass markers or apparent protein molecular masses (indicated by ~) are indicated in C and D in kilodaltons.

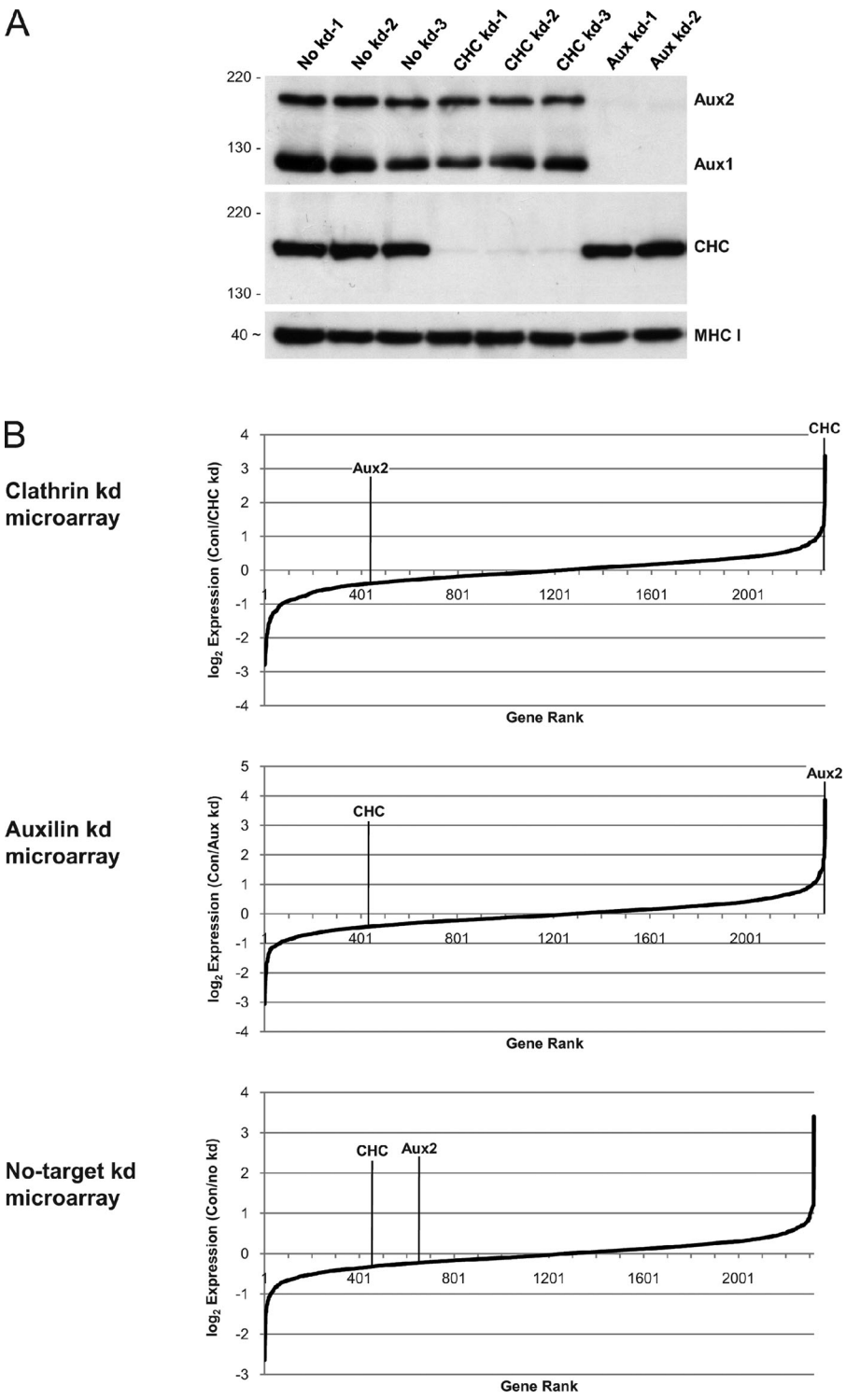

Figure S2. **Microarray gene expression analysis of clathrin- and auxilin-depleted cells.** The proteomic analyses presented in Figs. 1 and 2 indicate numerous substantial changes at the protein level in response to siRNA-mediated knockdown of clathrin or auxilin. To test if any of these changes were the result of altered gene expression, a genome-wide microarray-based assay was performed. HeLa cells were treated with siRNA against CHC, auxilin 1 and 2 (Aux), or with a nontargeting siRNA. Each treatment was performed in triplicate (duplicate for auxilin knockdown). Untreated control cells were grown in SILAC medium (not depicted). (A) Western blot analysis of whole cell lysates to test the knockdown efficiency. No kd 1–3, nontarget siRNA treatments; CHC kd 1–3, clathrin knockdowns; Aux kd 1–2, auxilin (1 and 2) knockdowns. Depletion of clathrin or auxilin (isoforms 1 and 2) was highly effective and specific. MHC-I is shown as a loading control. Positions of protein molecular mass markers or apparent protein molecular masses (indicated by ~) are indicated in kilodaltons. (B) Microarray analysis. Gene expression was assayed by detecting mRNA levels with a genome-wide microarray. The mean signal was calculated for each gene under each treatment. In cases where multiple probes targeted the same gene, the probe with the most significant change was chosen. Only the genes corresponding to the 2,527 proteins detected in the CCV fraction (Table S1) were considered for further analysis. The microarray analysis covered >2,300 of these (>91%). For each siRNA treatment, a binary comparison with control cells was performed by calculating the $\log_2$ of the ratio (control/siRNA treated). Genes were sorted from the lowest to the highest ratio, and plotted. A log ratio of 0 corresponds to no change, a ratio of 1 to a twofold change, a ratio of 2 to a fourfold change, and a ratio of 3 to an eightfold change. Positive log ratios signify depletion in the treated cells relative to control cells; negative ratios indicate an increase in expression. Under each of the three conditions, the vast majority of genes showed no or very small changes in expression (log ratio close to 0), which suggests that the knockdowns had very low levels of off-target effects. A small proportion of genes showed more substantial changes. As expected, these included clathrin and auxilin in their respective knockdowns, demonstrating that the experimental setup is suitable to detect large changes in gene expression. In agreement with the Western blot data (A), expression of clathrin in the auxilin knockdown was unaltered, as was expression of auxilin in the clathrin knockdown. Neither auxilin nor clathrin expression were substantially affected in the nontargeting knockdown. The positions of clathrin and auxilin 2 are indicated in each plot (auxilin 1 expression was not covered by the microarray data). To ensure a stringent analysis of our proteomic data, any gene whose expression was changed more than threefold (log ratio > 1.58 or < −1.58) by one or more of the knockdown conditions was excluded from further analysis (32 out of ~2,300 genes, indicated in Table S1; clathrin and auxilin were not excluded).

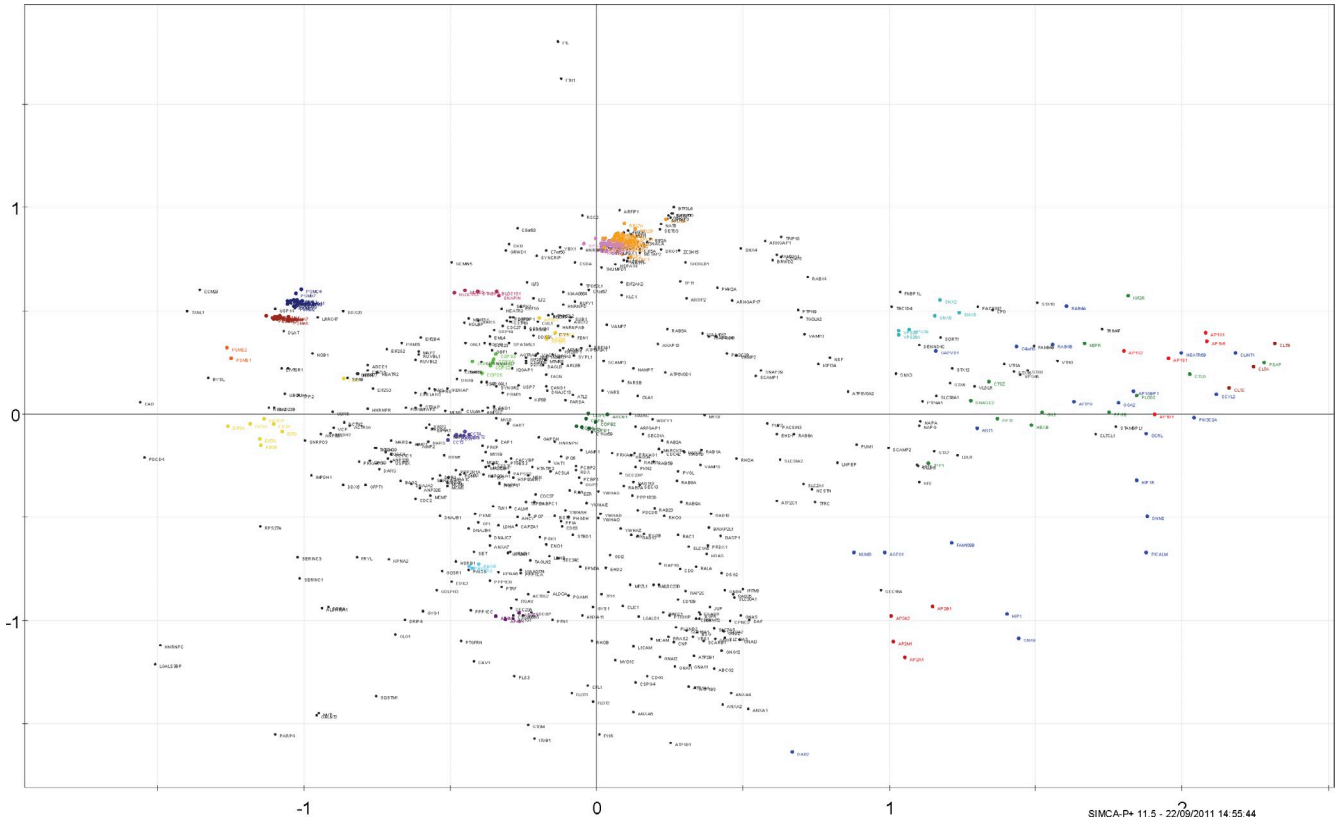

Figure S3. **PCA reveals clustering of CCV and non-CCV proteins into functional groups.** This figure is a fully annotated version of Fig. 3. CCV-enriched fractions were prepared under different experimental conditions, and compared by quantitative mass spectrometry. In total, 10 binary comparisons (CCV fraction from treated cells vs. control CCV fractions) were performed, and subjected to PCA. Projections of the data on the first (x axis) and second (y axis) principal components are shown (scores plot). Proximity of proteins indicates similar profiles, and hence suggests a potential functional association. UniProt gene names are used as unique protein identifiers (http://www.uniprot.org). It is recommended to view this figure on-screen, and to zoom in on areas of interest. Proteins that are subunits of a known complex are shown in the same color (see also Fig. 3). Clathrin adaptors AP-1 and AP-2 are separated from non-CCV proteins, and cluster with known CCV accessory coat components (shown in blue). Lysosomal enzymes and lysosomal sorting receptors (M6PR) are known cargo molecules of AP-1 vesicles (shown in green). Gray scatter points in the vicinity of AP-1 or AP-2 correspond to candidate new CCV proteins. The discriminating power of the analysis is highest for peripheral proteins. Central clusters are likely to be merged with functionally unrelated proteins. Furthermore, the first and second principal components together account for only ~76% of the variability in the data ($R^2_{cumulative}$ = 0.76). Higher order components confer greater capacity to discriminate between clusters, but the associated multidimensional projection is rendered impractical to illustrate in print for large datasets. Hence, it is important to note that close or superimposed proteins in the illustration may be further separated by the third or fourth principal components. The AP-4 cluster is an example of this (see Fig. S4). Only the 688 proteins common to all 10 SILAC datasets are shown. For the complete CCV profiling analysis, cluster assignment of proteins was performed in the context of a reference set, using automated PCA. For the accurate determination of the nearest cluster, candidate data were projected on more than two principal components, and distance measurements were performed in multidimensional space (see main text and Materials and methods for details).

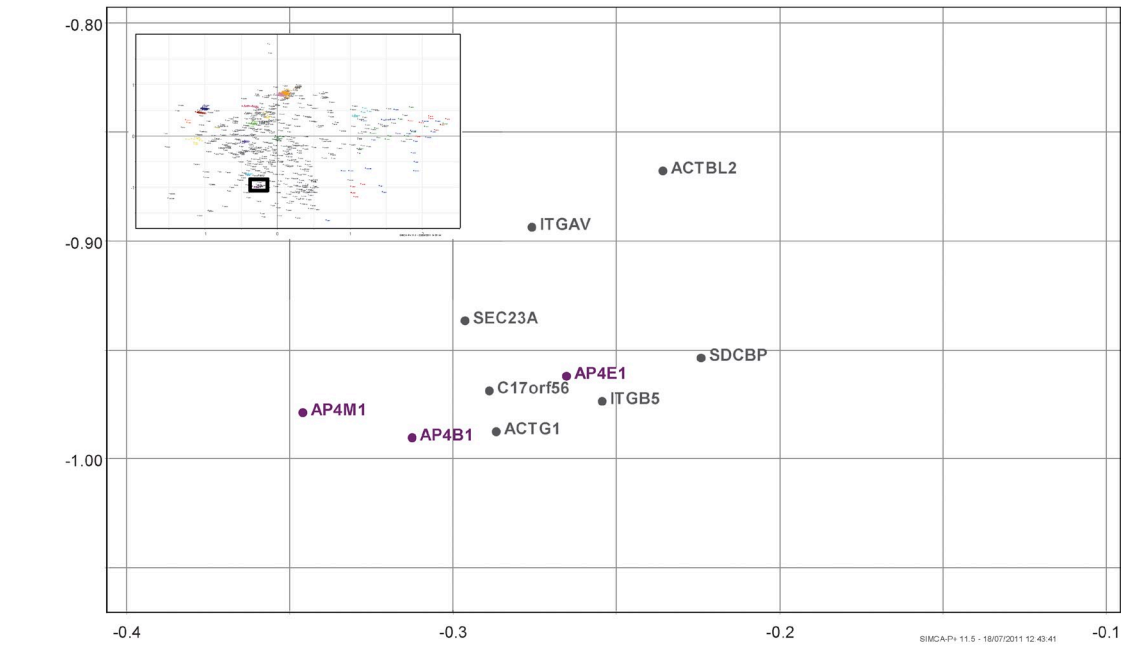

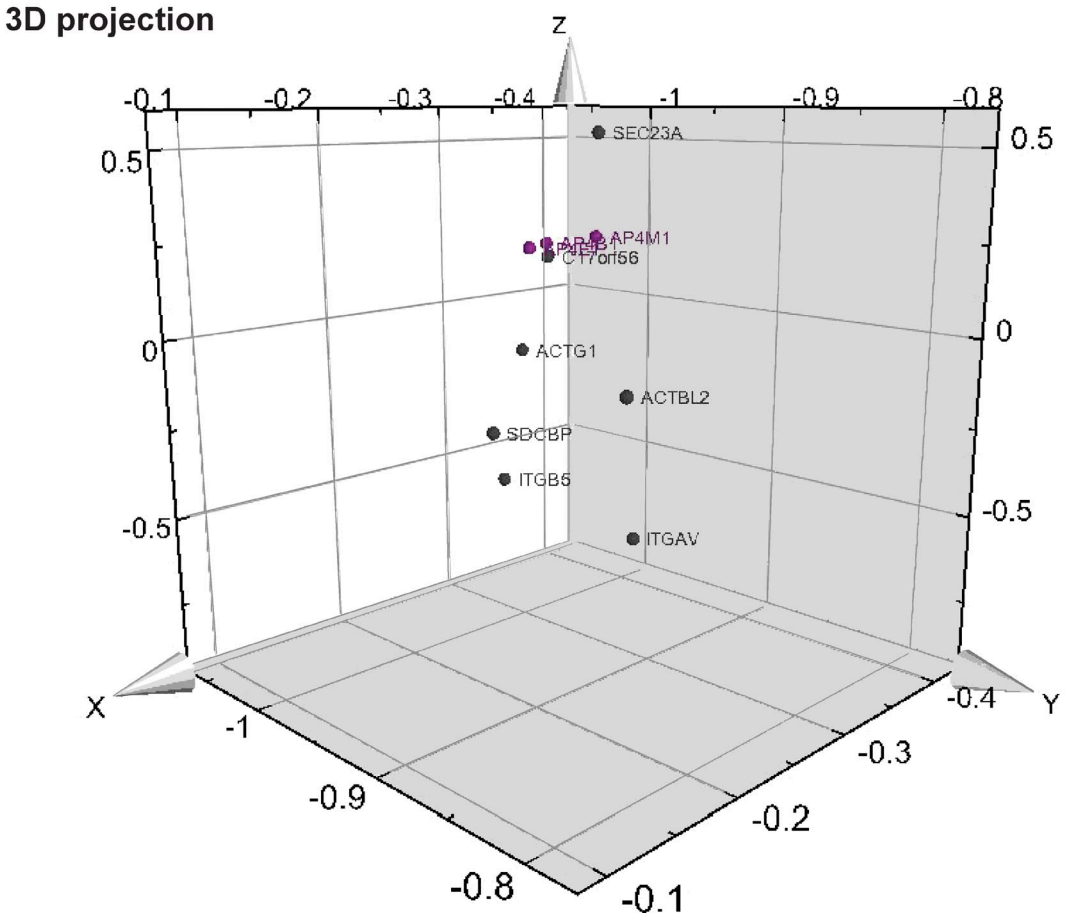

Figure S4. **A three-dimensional PCA scores plot reveals a novel candidate AP-4–associated protein.** The two-dimensional plot is a magnified section from Fig. S3 (as indicated in the inset), showing the AP-4 complex (shaded in purple) and the surrounding area. X and y axes correspond to the projections on the first and second principal components, respectively. Several proteins appear to cluster with the AP-4 subunits. However, a three-dimensional projection on the first three principal components reveals that although the AP-4 subunits and C17orf56 form a very tight cluster, they are clearly separated from the other proteins by the third principal component (z axis). C17orf56 is the only strong candidate AP-4–associated protein.

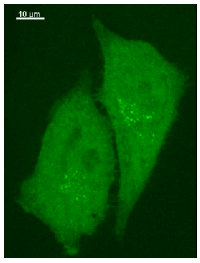

Video 1. **Tepsin-GFP puncta are highly mobile.** HeLa cells stably expressing tepsin-GFP were analyzed by time-lapse confocal microscopy using a spinning disk microscope (Cell Observer; Carl Zeiss). A z stack of five optical sections (thickness = ~1 µm/slice) was imaged every 2.6 s over a period of 175 s. Z stacks were collapsed into maximum intensity projections, and rendered at 15 frames per second (accelerated ~40×).

References

Borner, G.H., M. Harbour, S. Hester, K.S. Lilley, and M.S. Robinson. 2006. Comparative proteomics of clathrin-coated vesicles. *J. Cell Biol.* 175:571–578. http://dx.doi.org/10.1083/jcb.200607164

Hirst, J., S.E. Miller, M.J. Taylor, G.F. von Mollard, and M.S. Robinson. 2004. EpsinR is an adaptor for the SNARE protein Vti1b. *Mol. Biol. Cell*. 15:5593–5602. http://dx.doi.org/10.1091/mbc.E04-06-0468

Tables S1–S4 are provided as Microsoft Excel files.

Table S1 shows the complete proteomic profiling data. All 2,527 proteins identified in the CCV fraction are listed here, including their corresponding ratio and peptide count data.

Table S2 shows predicted CCV proteins. A detailed summary of the results of the profiling analysis is given.

Table S3 shows predicted clathrin cage–associated proteins.

Table S4 shows the dataset and a step-by-step guide to recreating Fig. 3 (PCA).